Electrochimica Acta 122 (2014) 180–186

Contents lists available at ScienceDirect

Electrochimica Acta

journal homepage: www.elsevier.com/locate/electacta

$LiFe_{1-x}M^{II}_xPO_4/C$ (M^{II} = Co, Ni, Mg) as cathode materials for lithium-ion batteries

Svetlana Novikova[a,*], Sergey Yaroslavtsev[b], Vyacheslav Rusakov[b], Tatyana Kulova[c], Alexander Skundin[c], Andrey Yaroslavtsev[a,b]

[a] Kurnakov Institute of General and Inorganic Chemistry, Russian Academy of Science, Leninsky pr. 31, Moscow, Russia
[b] Lomonosov Moscow State University, Leninsky gory 1, Moscow, Russia
[c] Frumkin Institute of Physical Chemistry and Electrochemistry, Russian Academy of Sciences, Leninsky pr. 31, Moscow, Russia

ARTICLE INFO

Article history:
Received 30 June 2013
Received in revised form 20 August 2013
Accepted 21 August 2013
Available online 1 September 2013

Keywords:
Cathode materials
Lithium ion battery
Lithium iron phosphate
Rate capability
Mössbauer spectroscopy

ABSTRACT

$LiFe_{1-x}M^{II}_xPO_4/C$ (M^{II} = Co, Ni, Mg) composites had been obtained by sol–gel method. Structure and morphology of the obtained materials have been studied with the use of the XRD-analysis, SEM and Mössbauer spectroscopy. Their electrochemical behavior has been investigated with the use of charge/discharge tests. The materials doped by cobalt and nickel were shown to be characterized by an increased lithium intercalation and deintercalation rates, and retain a high capacity during charge and discharge the battery at high currents densities ($LiFe_{0.9}Ni_{0.1}PO_4$ capacity amounts to 145 and 62 mAh/g at a discharge current 50 and 3000 mA/g). Mg^{2+} incorporation into $LiFePO_4/C$ cathode material results in the slight increase of charge/discharge rate and significant capacity decrease. Mössbauer spectroscopy has shown that M^{II} ions in the $LiFe_{1-x}M^{II}_xPO_4/C$ (M^{II} = Co, Ni) materials are orderly distributed both in charged and discharged states, each iron ion has no more than one M^{II} ion in the nearest environment. In the case of Ni-doped samples the ordering is less pronounced. The reasons of the changes observed in the electrochemical performances and charge/discharge rate have been discussed on the base of Mössbauer spectroscopy and XRD data.

1. Introduction

Nowadays cathode materials for lithium-ion batteries (LIBs) should meet such requirements as safety, high capacity, rate capability and low cost. $LiFePO_4$ based cathode materials satisfy the most of these requirements [1–5]. The anion sublattice of this material is characterized by the structural and chemical stability. The lithiated ($LiFePO_4$) and delithiated ($FePO_4$) forms are of similar structure, but have low mutual solubility [6]. This ensures short charge/discharge voltage range (approximately 3.5 V) and relatively lower oxidability of electrolyte components in LIBs [7]. In the case of $LiFePO_4$ particles coated with carbon the rate of charge and discharge processes is limited by the ion conductivity of the material [6,8]. The improvement of cathode materials performance at high rates is an important problem for a wide variety of applications of the LIBs. Such approaches as minimization of particle size or ion conductivity enhancement by heterovalent doping can be used in order to improve ion conductivity. These approaches use can lead to the additional point defects formation in the surface layer or in the bulk of the solid electrolytes and as a result to the ion conductivity increase [9–13]. Cathode materials modification with the help of techniques mentioned above leads to the improvement of power density with maintaining a relatively high capacity in some cases [14–19].

So the main goal of this work was to study the electrochemical properties of materials $LiFe_{1-X}M_XPO_4$ (M = Co, Ni, Mg) coated with a thin carbon layer and to describe the ordering processes that take place during electrochemical lithium intercalation/deintercalation.

2. Experimental

$LiFePO_4$-based composite materials coated with thin carbon layer were prepared by a sol–gel process described elsewhere [6]. The samples $LiFe_{1-x}M^{II}_xPO_4/C$ (M^{II} = Co, Ni, Mg) were synthesized followed the same procedure by adding the appropriate amounts of $Co(NO_3)_2$, $Ni(NO_3)_2$ or $MgCO_3$ into the reaction mixture instead of $Fe(NO_3)_3$. The degree of iron substitution for M^{II} varied from 0% to 20%. The carbon content in the obtained composite materials was determined from the weight of the residue after calcination at 970 K for 3 h.

Crystal structure was characterized by X-ray diffraction (XRD) with Cu K_α radiation performed on a Rigaku D/MAX 2200

* Corresponding author at: Leninsky pr., Moscow 119991, Russia.
Tel.: +7 495 952 24 87; fax: +7 495 954 12 79.
E-mail address: novikova@igic.ras.ru (S. Novikova).

0013-4686/$ – see front matter © 2013 Elsevier Ltd. All rights reserved.
http://dx.doi.org/10.1016/j.electacta.2013.08.118

diffractometer. XRD data were analyzed using Rigaku Application Data Processing software.

Microstructures of obtained materials were examined with the help of the scanning electron microscope Carl Zeiss NVision 40.

Electrode paste was prepared by thoroughly mixing 85% $LiFe_{1-X}M^{II}_XPO_4$ (M = Co, Ni, Mg) as an active material, 10% conductive carbon black (Timcal, Belgium), and 5% binder (polyvinylidene fluoride (Aldrich) dissolved in anhydrous N-methyl-2-pyrrolidinone). The paste was applied to stainless steel gauze (electrical lead) as a 5 mg/cm^2 layer. The resultant electrode was pressed at 1000 kg/cm^2 and vacuum-dried at 120 °C for 8 h.

Electrochemical tests were performed in hermetically sealed three-electrode ($LiFe_{1-X}M^{II}_XPO_4$/Li/Li) cells. The area of the working electrode was 2.25 cm^2, and that of the auxiliary (lithium) electrode was 5 cm^2. The cells were assembled in a glove box under an argon atmosphere with a humidity level of <10 ppm. A nonwoven polypropylene separator (NPO Ufim, Moscow) was placed between electrodes. 1 M $LiPF_6$ solution in a mixture of ethylene carbonate, diethyl carbonate and dimethyl carbonate (Novolyte, USA) was used as electrolyte. Electrochemical cycling of the cells was performed at voltages range 2.5–4.1 V using a ZRU 50 mA–10 V charge–discharge system (OOO NTTs Buster, Russia). The tests were performed in galvanostatic mode at a currents densities of 15, 30, 60, 120, 240, 480, 960 mA/g. The samples containing the iron ions which have been partially or fully transformed into the Fe^{3+} state were obtained with the same electrochemical cell. The degree of $Fe^{2+} \leftrightarrow Fe^{3+}$ conversion was controlled by the measurements of the electrical charge passed. Thereafter, the cathode material was vacuum-dried and gently scraped from the current collector. The samples obtained by this way were investigated with the help of XRD analysis and Mössbauer spectroscopy.

Mössbauer spectra have been recorded using a constant-acceleration spectrometer MS-1101E of electromechanical-type with a ^{57}Co source in a rhodium matrix. The spectrometer was calibrated by the use of a standard α-Fe sample at room temperature. Low temperature spectra have been obtained with the help of the helium cryostat SHI-850-5 from JANIS RESEARCH. The Mössbauer parameters were obtained by least squares fitting program SpectrRelax [20].

3. Results and discussion

3.1. Structure and morphology

The XRD pattern of prepared $LiFe_{1-x}M^{II}_xPO_4$/C (M^{II} = Co, Ni, Mg; x = 0–0.2) materials have shown that all materials obtained are presented by single crystal phase and indexed in orthorhombic syngony (Fig. 1). According to the TGA data all the samples obtained contain ~4 wt% of amorphous carbon. Two phases ($FePO_4$ and $LiFePO_4$) present in the samples with intermediate charge/discharge level. Moreover, the second phase can be clearly indicated already when 5% of Fe^{2+} ions are located in $FePO_4$ or 5% of Fe^{3+} ions are located in $LiFePO_4$.

The unit cell parameters of crystal lattice change regularly for doped samples (Fig. 2) that proves solid solution formation.

According to XRD data the mean size of X-ray coherent scattering regions for all samples investigated is about 50 nm. While electron microscopy data have shown that for M^{II}-doped samples the aggregation of the particles is observed. This effect is the most pronounced in the case of Mg^{2+} ions incorporation and the less pronounced for $LiFe_{1-X}Ni_XPO_4$. For example, for cobalt doped samples the particle size increase from 260 nm up to 320 nm with cobalt concentration increase from 2% to 20%. X-ray microanalysis data have shown that the M^{II} content in the samples corresponds to the loaded one.

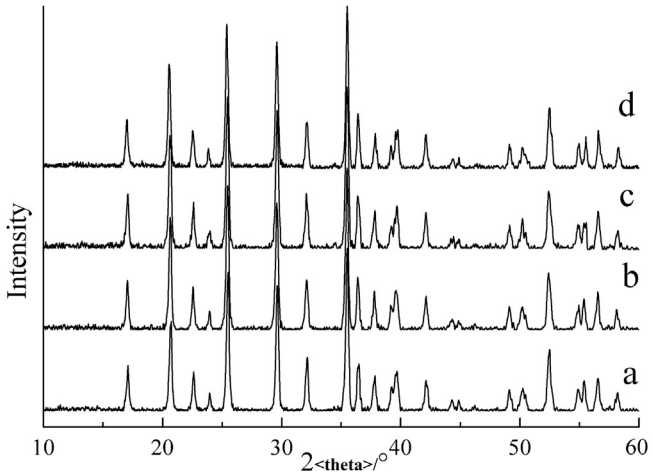

Fig. 1. The XRD patterns of $LiFePO_4$ (a), $LiFe_{0.9}Mg_{0.1}PO_4$ (b), $LiFe_{0.9}Co_{0.1}PO_4$ (c), $LiFe_{0.9}Ni_{0.1}PO_4$ (d).

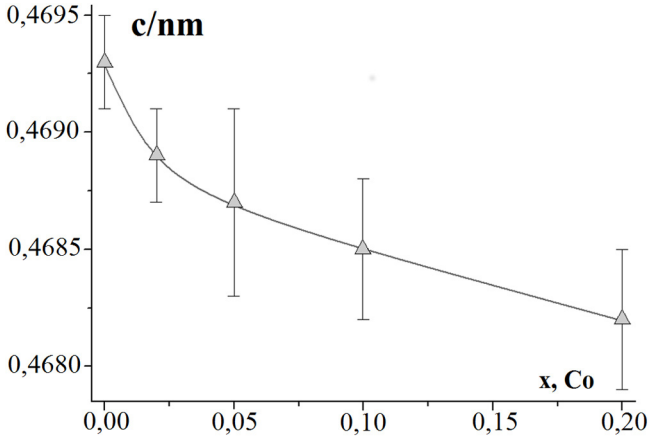

Fig. 2. Effect of cobalt content on the "c" parameter of the unit cell of $LiFe_{1-X}Co_XPO_4$.

3.2. Charge/discharge behavior

Magnesium ions have a sole oxidation state 2+. On the other hand, the voltage for redox couples Co^{2+}/Co^{3+} and Ni^{2+}/Ni^{3+} is much higher than that for the Fe^{2+}/Fe^{3+} couple [21]. Therefore, Co^{2+} and Ni^{2+} ions will not take part in electrochemical processes at potentials corresponding to the $LiFePO_4$ charge. From this point of view, one can suppose that doping of $FePO_4$ sample by divalent cations can lead to its ion conductivity increase. Lithium transfer in the Fe^{3+} containing phase determines the rate of charge processes in LIBs. Therefore, the acceleration of the battery charge process can be expected (Fig. 3).

Figs. 4 and 5 represent charge and discharge curves for $LiFe_{0.9}M^{II}_{0.1}PO_4$/C ($M^{II}$ = Co, Ni, Mg) samples under the current density as low as 15 mA/g (C/10). The charge/discharge curves for undoped and doped samples have practically the same shape with a voltage plateau about 3.5 V that is typical for $LiFePO_4$ cathode materials. It is worth noting that average operating voltage of LIBs remains almost unchanged after partial iron substitution by Mg^{2+}, Co^{2+}, Ni^{2+} ions. This indicates that the capacity of the cathode material under operating in the range of 2.5–4.2 V is determined only by Fe^{2+}/Fe^{3+} couple. On the other hand the charge processes for doped materials are characterized by slightly lower potential values, while discharge processes – by slightly higher potential values compared with $LiFePO_4$/C (Table 1). This indicates that energy losses during charge/discharge cycles decrease by 40–70%. This effect can be

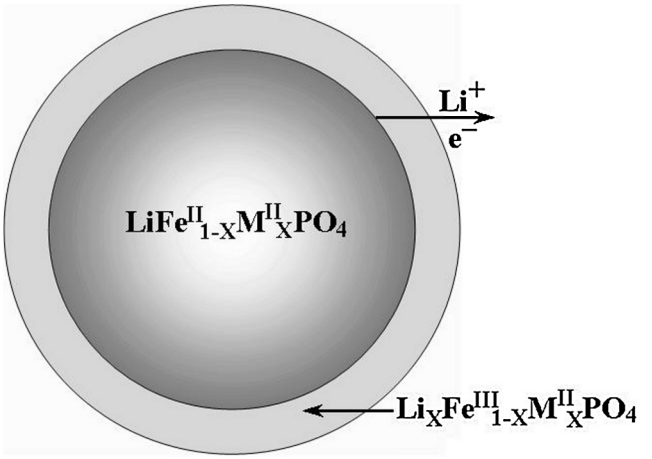

Fig. 3. Scheme of electron/lithium extraction from $LiFe_{1-X}M^{II}{}_XPO_4$ according to the heterogeneous grain model.

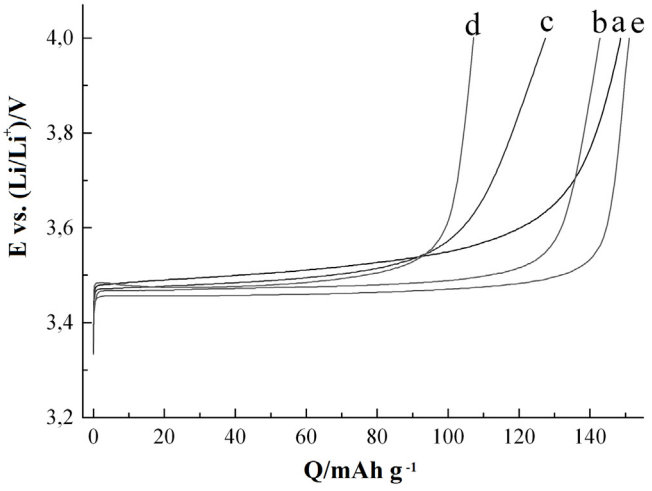

Fig. 4. Charge curves under 15 mA/g (C/10) for the $LiFePO_4$ (a), $LiFe_{0.98}Co_{0.02}PO_4$ (b), $LiFe_{0.9}Co_{0.1}PO_4$ (c), $LiFe_{0.9}Mg_{0.1}PO_4$ (d), $LiFe_{0.9}Ni_{0.1}PO_4$ (e).

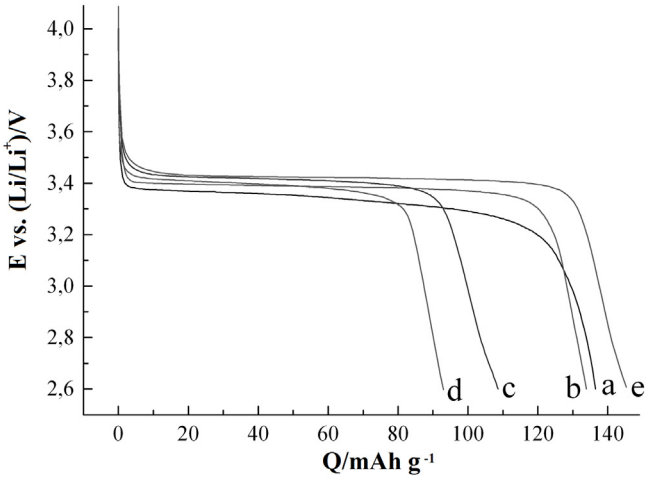

Fig. 5. Discharge curves under 15 mA/g (C/10) for the $LiFePO_4$ (a), $LiFe_{0.98}Co_{0.02}PO_4$ (b), $LiFe_{0.9}Co_{0.1}PO_4$ (c), $LiFe_{0.9}Mg_{0.1}PO_4$ (d), $LiFe_{0.9}Ni_{0.1}PO_4$ (e).

Table 1
Charge and discharge potentials of $LiFe_{1-x}M^{II}{}_xPO_4$ (M^{II} = Co, Ni, Mg) samples vs. Li/Li^+.

Composition	Charge potential (E_{charge}), V	Discharge potential ($E_{discharge}$), V	$E_{charge} - E_{discharge}$, V
$LiFePO_4$/C	3.50	3.34	0.16
$LiFe_{0.9}Mg_{0.1}PO_4$/C	3.47	3.40	0.07
$LiFe_{0.98}Co_{0.02}PO_4$/C	3.47	3.38	0.09
$LiFe_{0.9}Co_{0.1}PO_4$/C	3.48	3.40	0.08
$LiFe_{0.9}Ni_{0.1}PO_4$/C	3.46	3.42	0.04

caused by the decrease of the resistance of the cathode material particles (Fig. 3). However, in the case of magnesium-containing samples the resulting resistance is almost the same but the effect remains. Therefore, the overvoltage decrease can be considered as the most probably reason of the decrease of the difference between charge and discharge voltage for metal-doped samples. The overvoltage decrease, in its turn, can be explained by the changes in the conditions of lithium ions transfer between $LiFePO_4$ and $FePO_4$ or $LiFePO_4$ ($FePO_4$) and C phases.

Two important features of charge/discharge processes should be noted from data presented in the Figs. 4 and 5. The first one is that the slope of the voltage plateau for doped samples is lower than that for undoped $LiFePO_4$. This fact indicates that cations M^{II} incorporation into $LiFePO_4$ results in the charge/discharge rate increase. In the case of magnesium doped samples the charge/discharge rate increase is less pronounced in comparison with cobalt and nickel incorporation. The second feature is that the charge/discharge capacity of cobalt and magnesium containing samples decreases with the dopant concentration increase over 15 mA/g (C/10) (Figs. 4 and 5). Its important to note that for all samples with high dopant concentration, including $LiFe_{0.8}Ni_{0.2}PO_4$, the charge/discharge capacity decreases drastically.

The decrease of discharge capacity takes place due to the decrease in the iron content in the doped samples. The charge of LIB within standard range of potentials for $LiFePO_4$ based materials (2.5–4.2 V) leads to the formation of cathode materials with the composition $Li_X(Fe^{III})_{1-X}(M^{II})_XPO_4$. As a result the partial deintercalation of lithium and decrease of charge and discharge capacity are observed. But in the case of $Li_X(Fe^{III})_{0.9}(M^{II})_{0.1}PO_4$ samples the charge capacity reduces by 15% for cobalt-containing material, and by 30% for magnesium-containing material. This could be explained by the increase in the particles size. However, for the $LiFe_{0.98}Co_{0.02}PO_4$ sample the particle size is only slightly smaller than for the samples with a high cobalt content but the deviation of observed capacity from the calculated one is significantly less and the rate of the charge/discharge processes is higher. At the same time for $LiFe_{0.9}Ni_{0.1}PO_4$ sample the capacity is close to the theoretically calculated value and it is equal to the capacity of undoped $LiFePO_4$.

Deintercalation/intercalation of lithium ions during charge/discharge of LIB with $LiFePO_4$ based cathode takes place by means of the heterogeneous grain model (Fig. 3). The charge/discharge rate is limited by the lithium diffusion in the forming shells of the cathode material particles and depends strongly on the particle size [6]. The observed charge/discharge rate increase after $LiFePO_4$ doping by M^{II} is caused by the ion conductivity increase of the forming shell of the cathode material particles.

$LiFe_{0.95}Co_{0.05}PO_4$ is characterized by the highest charge rate and accordingly by the highest lithium diffusion coefficient among the $Li_xFe^{III}{}_{1-x}Co_xPO_4$ samples. This fact seems to be rather unexpected. Lithium diffusion coefficient depends on the defects concentration. Each cobalt ion embedded into charged $Li_xFe^{III}{}_{1-x}Co_xPO_4$ form leads to the introduction of the interstitial lithium ions into the $FePO_4$ structure and therefore charge carrier concentration

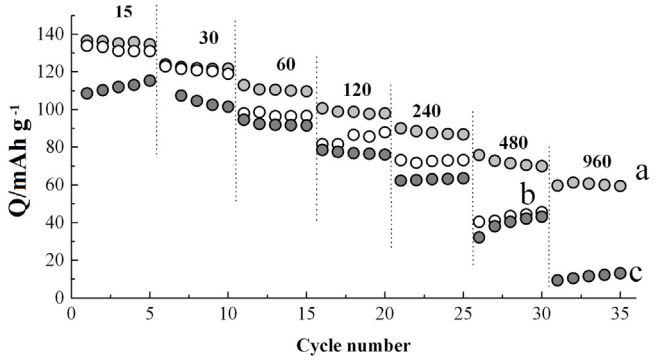

Fig. 6. Discharge capacity vs. number of cycles during cycling under various current densities (15–960 mA/g, $i_{charge} = i_{discharge}$) for $LiFePO_4$ (a), $LiFe_{0.98}Co_{0.02}PO_4$ (b), $LiFe_{0.9}Co_{0.1}PO_4$ (c). Current density values (mA/g) are given in the figure.

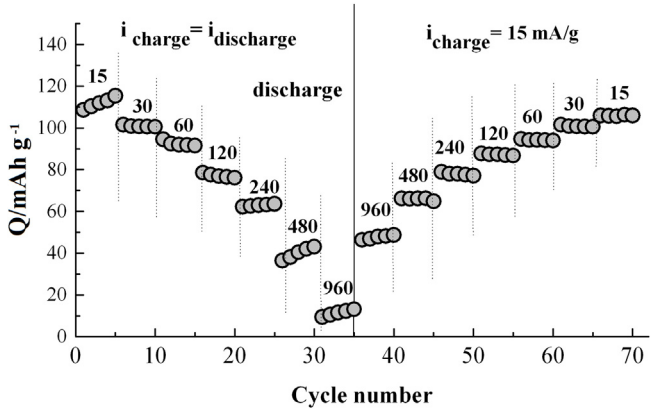

Fig. 7. Discharge capacity as a function of current density during cycling under various current densities for $LiFe_{0.9}Co_{0.1}PO_4$. Current density values (mA/g) are given in the figure.

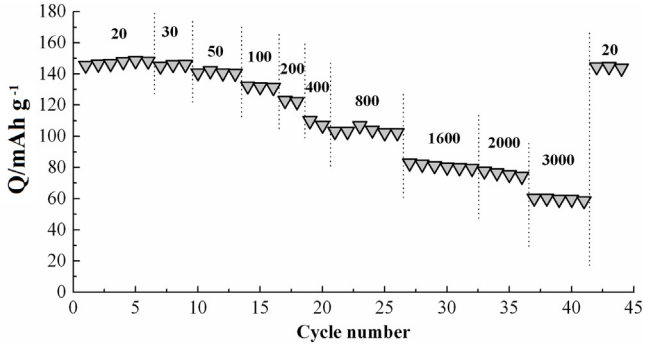

Fig. 8. Discharge capacity dependence on number of cycles under various current densities (15–960 mA/g, $i_{charge} = i_{discharge}$) for $LiFe_{0.9}Ni_{0.1}PO_4$. Current density values (mA/g) are given in the figure.

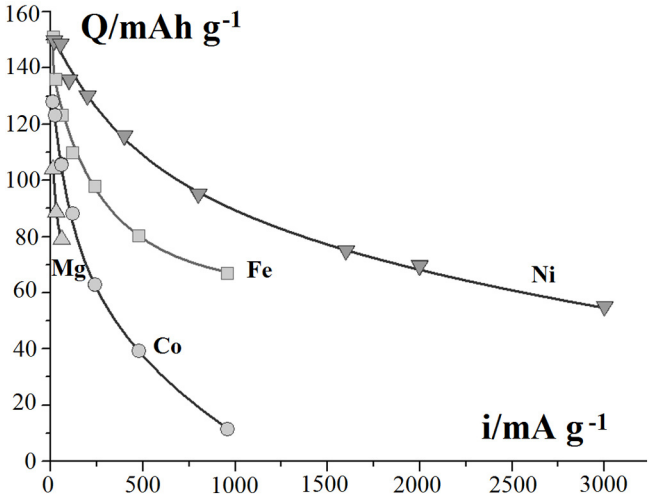

Fig. 9. Discharge capacity vs. current density for $LiFe_{0.9}M^{II}_{0.1}PO_4$ (M^{II} = Co, Ni, Mg).

increases. At the same time it is known that defect association processes usually take place in solid electrolytes [13,22]. It is reasonable to assume that the $LiFe_{0.9}Co_{0.1}PO_4$ sample contains ion pairs, such as $[(Co^{2+})'(Li^{+}_{i})^{*}]$ in which the Co^{2+} ions have a negative charge relative to its position in $FePO_4$ lattice and the lithium interstitials have a positive charge. This reduces the defects concentration. Moreover, defect centers can also reduce the carrier mobility, playing the role of traps.

Another unexpected fact is that discharge rate increases were observed too (Fig. 5). The reasons for this phenomenon are not quite clear, but we can assume that this is caused by the disordering of crystal lattice or by the local changes of the interatomic distances as a result of M^{II} ions incorporation into $LiFePO_4$ structure. This can leads to the facilitation of the defect formation processes.

Despite the fact that the charge/discharge rate increases the charge/discharge capacities for Co-doped samples decrease significantly under high current densities (Fig. 6). This reduction is reversible and capacity restores completely after the charging under low current density. Moreover, the discharge capacity for the sample charged under low current density (i_{charge} = 15 mA/g) is higher than that for the sample charged under high current densities (Fig. 7). This indicates that only the kinetic restrictions of transport processes are the reasons of discharge capacity decrease.

$LiFe_{0.9}Ni_{0.1}PO_4$ is characterized by the best electrochemical performances. Both charge and discharge maximum rates and significant increase in the charge/discharge capacity at high current densities has been achieved for the $LiFe_{0.9}Ni_{0.1}PO_4$ sample in comparison with initial $LiFePO_4$ (Figs. 8 and 9). The discharge capacity of $LiFe_{0.9}Ni_{0.1}PO_4$ is 62 mAh/g even at current density of 3000 mA/g (20 C). The discharge capacity of the initial $LiFePO_4$ as well as of Co- and Mg-doped samples decrease sharply with the current density increase.

It should be noted that despite the higher charge/discharge rate for Co-doped samples, their electrochemical capacity is worse than that for undoped $LiFePO_4$ for high current densities. The formation of the clusters with high cobalt ion concentrations near the centers of the particles during charge of cathode material can be considered as a possible reason for this phenomenon. Such assumption was made by us in [16] and it based on the low mutual solubility of $LiFePO_4$ and $FePO_4$. The metal-doped samples were investigated with the help of Mossbauer spectroscopy for verification of this hypothesis (see Section 3.3).

Magnesium doping leads to largest charge/discharge capacity decrease (Figs. 4 and 5). The obtained results in the case of cobalt, nickel and magnesium doped materials can be explained in terms of different doping mechanisms. Cobalt and nickel substitute iron ions while magnesium ions can be incorporated both into Fe^{2+} and Li^{+} positions.

3.3. *Mössbauer spectroscopy*

Mössbauer spectra for all of the studied samples at 5 K are characterized by hyperfine magnetic structures (Figs. 10a and 11a). These spectra were analyzed with the full Hamiltonian for the ^{57}Fe nucleus, including both the magnetic dipole and the electric quadrupole interaction. At the same time, the reconstruction of the hyperfine field distributions $p(H_n)$ (Figs. 10b and 11b) was carried

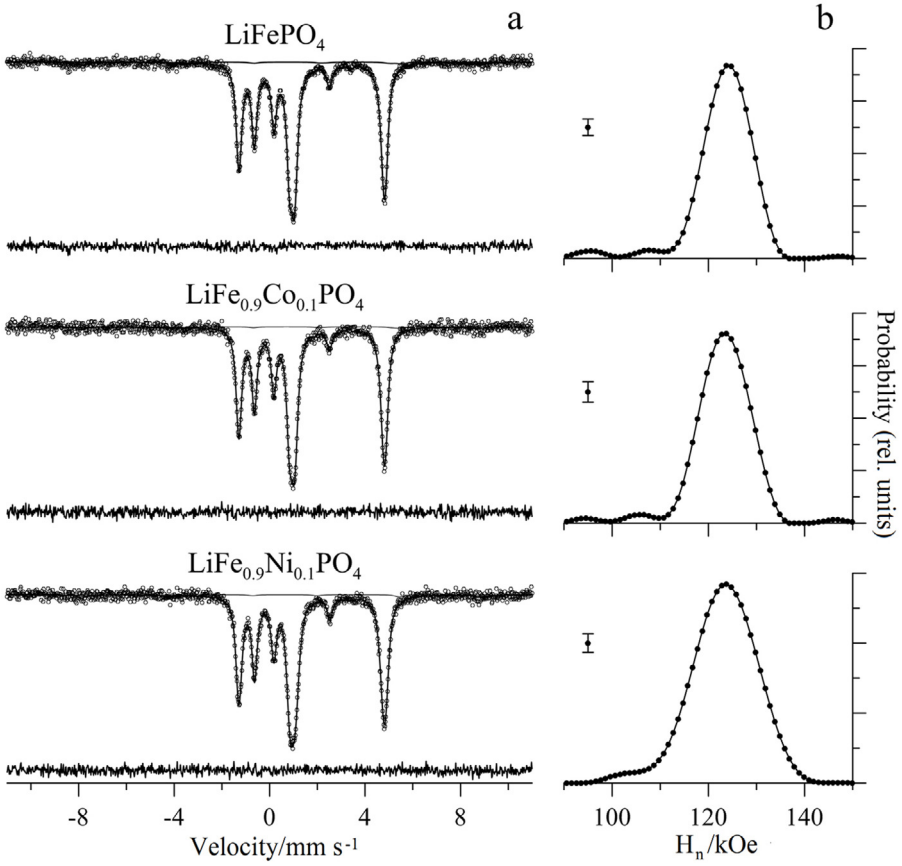

Fig. 10. Mössbauer spectra (a) and corresponding hyperfine magnetic field distributions (b) for $LiFePO_4$, $LiFe_{0.9}Co_{0.1}PO_4$ and $LiFe_{0.9}Ni_{0.1}PO_4$ at 5 K. Maximum standard deviations are presented on the left of (b).

out with the use of the SpectrRelax program in the case of a linear correlation between all of the hyperfine spectrum parameters [20].

$LiFePO_4$ has a spectrum (Fig. 10) with hyperfine parameters typical for divalent iron ions: isomer shift $\delta = 1.351 \pm 0.003$ mm/s, quadrupole coupling constant $e^2qQ = 5.527 \pm 0.013$ mm/s, and magnetic hyperfine field $H_n = 123.1 \pm 0.4$ kOe. The hyperfine parameters for $FePO_4$ (Fig. 11) have values characteristic for trivalent iron ions: $\delta = 0.543 \pm 0.004$ mm/s, $e^2qQ = -2.725 \pm 0.035$ mm/s, and $H_n = 501.1 \pm 0.2$ kOe. These values correspond to the maximum value of the probability distribution $p(H_n)$. At the same time the small contribution to the each spectrum from the iron atoms with other valence can be observed.

Cobalt or nickel doping does not change the Mössbauer $LiFePO_4$ spectrum (Fig. 10). Much greater changes are observed for $Li_{0.1}Fe_{0.9}Co_{0.1}PO_4$ and $Li_{0.1}Fe_{0.9}Ni_{0.1}PO_4$ spectra (Fig. 11), where the resonance lines are broadened and change their amplitudes noticeably.

The restored distribution of the hyperfine magnetic field $p(H_n)$ for $Li_{0.1}Fe_{0.9}Co_{0.1}PO_4$ (Fig. 11b) shows that its spectrum is a superposition of two subspectra, the first of which has a relative intensity of $55 \pm 1\%$ and practically matches the spectrum of undoped $FePO_4$. Whereas the second one has hyperfine parameters $\delta = 0.567 \pm 0.004$ mm/s, $e^2qQ = -0.77 \pm 0.16$ mm/s, $H_n = 517.7 \pm 1.5$ kOe, and an intensity of $45 \pm 1\%$. The environment of each iron ion in $LiFePO_4$ and $FePO_4$ structures contains four ions of the same kind having common vertices of the coordination polyhedra. If cobalt ions are randomly distributed in iron positions, 65.61% of iron ions in $Li_{0.1}Fe_{0.9}Co_{0.1}PO_4$ should have only iron ions as the nearest neighbors, 29.16% should have one cobalt atom, 4.86% - two cobalt ions and 0.36 and 0.01% – 3 or 4 cobalt ions, respectively. Thus, depending on the quality of the Mössbauer spectrum, we might be able to record a few subspectra with an intensity ratio of ≈66:29:5 for the three most intense ones. If clusters with high Co^{2+} concentration were formed, the difference in the intensities of the subspectra would only increase. The observed intensities ratio of ≈55:45 can only be obtained in the case of ordered distribution of cobalt that should only be located in iron ion environments.

The fact that $LiFePO_4$ and $FePO_4$ phases have low mutual solubility means that, despite the similarity of these structures, the Fe^{3+} ions prefer to be surrounded by trivalent ions. From this point of view, it should be expected that the iron ions which have M^{II} ions in its nearest environment would pass to the trivalent state more slowly. It would be the most clearly seen in the case of the samples charged by about 50%. However according to the Mössbauer spectroscopy data the content of Fe^{3+} ions having one cobalt or nickel ion in the nearest environment is higher than 40%. The only one reasonable explanation for this phenomenon is that cobalt and nickel ions are distributed nonuniformly in the $Li_xFe_{1-x}M^{II}{}_xPO_4$ nanoparticles. Slightly larger amount of M^{II} are localized on the particle surface, where $FePO_4$ phase formation occurs (Fig. 3) according to the heterogeneous grains model [6].

It should be mentioned that analysis and interpretation of $Li_xFe_{0.9}Ni_{0.1}PO_4$ spectra are more difficult. These spectra in accordance with the result of reduction of $p(H_n)$ distribution (Fig. 11b) apparently contain several weak unresolved subspectra that may correspond to the nonequivalent positions of iron atoms with different number of nickel atoms in the nearest environment. It evidence in favor of the fact that these systems are less ordered.

So Mössbauer spectroscopy data disprove the hypothesis that clusters with a higher cobalt or nickel content would form during charge process. This probably caused by low divalent ions mobility in the $LiFe_{1-x}M_xPO_4$ structure. At the same time the

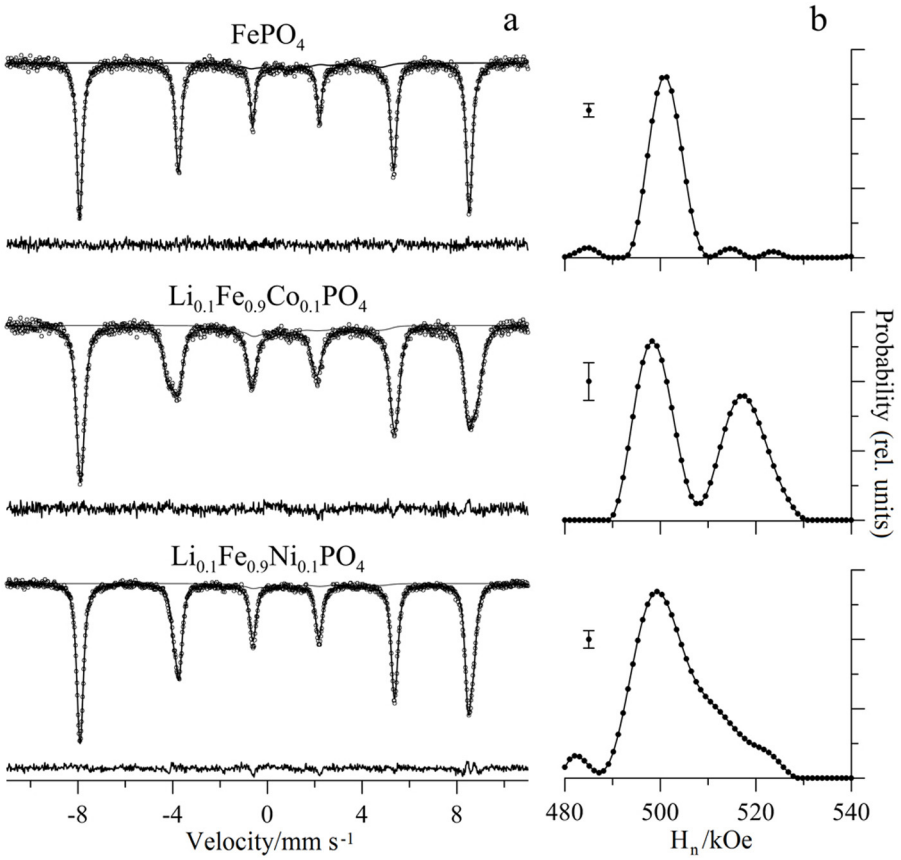

Fig. 11. Mössbauer spectra (a) and corresponding hyperfine magnetic field distributions (b) for $FePO_4$, $Li_{0.1}Fe_{0.9}Co_{0.1}PO_4$ and $Li_{0.1}Fe_{0.9}Ni_{0.1}PO_4$ at 5 K. Maximum standard deviations are presented on the left of (b).

phase separation into areas containing only two- or tricharged ions was not observed. New phase formation takes place during charge/discharge processes by means of heterogeneous nucleation mechanism – on the surface of the particles. This reduces the energy required for new phase formation at the interface significantly. Then the growth of a new phase in the interface occurs. In the case of Co- and Ni-doped samples this mechanism is also preferable in comparison with the small grains of a new phase formation with enhanced concentration of these metals.

However, in the last stages of charge for the Co-doped samples the process becomes complicated by energy coupling. This caused the ordering processes in the structure resulting in ordered cobalt ions distribution in the iron ions environment. For Ni-doped samples according to Mössbauer spectroscopy data the ordering process is less pronounced. This fact, coupled with a smaller aggregate size of $LiFe_{1-X}Ni_XPO_4$, determines the improvement of electrochemical performance of $LiFe_{0.9}Ni_{0.1}PO_4/C$ sample at high current densities compared with the Co-doped materials.

4. Conclusions

In this paper we successfully prepared $LiFe_{1-x}M^{II}{}_xPO_4/C$ (M^{II} = Co, Ni, Mg) composites by sol–gel method. It was shown that the materials doped by cobalt and nickel are characterized by an increased lithium intercalation and deintercalation rates, and retain a high capacity during the battery charge and discharge at high currents ($LiFe_{0.9}Ni_{0.1}PO_4/C$ capacity consists 145 and 62 mAh/g at a discharge current 50 and 3000 mA/g). Mg^{2+} incorporation into $LiFePO_4/C$ cathode material results in the strong capacity decrease. Mössbauer spectroscopy has shown that M^{II} ions in the $LiFe_{1-x}M^{II}{}_xPO_4/C$ (M^{II} = Co, Ni) materials are orderly distributed both in charged and discharged states, each iron ion has no more than one M^{II} ion in the nearest environment. Obtained results in the case of doped materials can be explained in terms of different doping mechanisms. We have assumed that cobalt and nickel substitute iron ions only while magnesium ions can occupy both Fe^{2+} and Li^+ positions in $LiFePO_4$ structure.

Acknowledgment

This work was supported by the Ministry of education and science of Russian Federation, project 8573.

References

[1] A.K. Padhi, K.S. Nanjundaswamy, J.B. Goodenough, Phospho-olivines as positive-electrode materials for rechargeable lithium batteries, J. Electrochem. Soc. 144 (1997) 144–1188.
[2] A. Veluchamy, C.-H. Doh, D.-H. Kim, J.-H. Lee, H.-M. Shin, B.-S. Jin, H.-S. Kim, S.-I. Moon, Thermal analysis of Li_xCoO_2 cathode material of lithium ion battery, J. Power Sources 189 (2009) 855.
[3] Z. Li, D. Zhang, F. Yang, Developments of lithium-ion batteries and challenges of $LiFePO_4$ as one promising cathode material, J. Mater. Sci. 44 (2009) 2435.
[4] J. Fergus, Recent developments in cathode materials for lithium ion batteries, J. Power Sources 195 (2010) 939.
[5] B. Scrosati, J. Garche, Lithium batteries: status, prospects and future, J. Power Sources 195 (2010) 2419.
[6] D.V. Safronov, S.A. Novikova, A.M. Skundin, A.B. Yaroslavtsev, Lithium intercalation and deintercalation processes in $Li_4Ti_5O_{12}$ and $LiFePO_4$, Inorg. Mater. 48 (2012) 57.
[7] N. Iltchev, Y. Chen, S. Okada, J. Yamaki, $LiFePO_4$ storage at room and elevated temperatures, J. Power Sources 119–121 (2003) 749.
[8] C. Benoit, S. Franger, Chemistry and electrochemistry of lithium iron phosphate, J. Solid State Electrochem. 12 (2008) 987.
[9] N.F. Uvarov, V.V. Boldyrev, Size effects in chemistry of heterogeneous systems, Russ. Chem. Rev. 70 (2001) 265.

[10] A.B. Yaroslavtsev, Composite materials with ionic conductivity: from inorganic composites to hybrid membranes, Russ. Chem. Rev. 178 (2009) 1013.
[11] J. Maier, Defect chemistry and ion transport in nano-structured materials. Part II. Aspects of nanoionics, Solid State Ionics 157 (2003) 327.
[12] J. Jamnik, J. Maier, Transport across boundary layers in ionic crystals. Part II. Stationary chemical diffusion, J. Phys. Chem. Solids 59 (1998) 1555.
[13] A.B. Yaroslavtsev, Ion conductivity of composite materials on the base of solid electrolytes and ion-exchange membranes, Inorg. Mater. 48 (2012) 1193.
[14] D. Wang, H. Li, S. Shi, X. Huang, L. Chen, Improving the rate performance of $LiFePO_4$ by Fe-site doping, Electrochim. Acta 50 (2005) 2955.
[15] M.R. Roberts, G. Vitins, J.R. Owen, High-throughput studies of $Li_{1-x}Mg_{x/2}FePO_4$ and $LiFe_{1-y}Mg_yPO_4$ and the effect of carbon coating, J. Power Sources 179 (2008) 754.
[16] D.V. Safronov, S.A. Novikova, T.L. Kulova, A.M. Skundin, A.B. Yaroslavtsev, Lithium diffusion in materials based on $LiFePO_4$ doped with cobalt and magnesium, Inorg. Mater. 48 (2012) 513.
[17] L. Wu, X. Li, Zh. Wang, X. Wang, L. Li, J. Fang, F. Wu, H. Guo, Preparation of synthetic rutile and metal-doped LiFePO4 from ilmenite, Powder Technol. 199 (2010) 293.
[18] T. Nakamura, Y. Miwa, M. Tabuchi, Y. Yamada, Structural and surface modifications of $LiFePO_4$ olivine particles and their electrochemical properties, J. Electrochem. Soc. 153 (6) (2006) A1108.
[19] D. Yan-huai, Zh. Ping, Effect of Mg and Co co-doping on electrochemical properties of $LiFePO_4$, Trans. Nonferrous Met. Soc. Chin. 22 (2012) s153.
[20] M.E. Matsnev, V.S. Rusakov, SpectrRelax, An application for Mössbauer spectra modeling and fitting, AIP Conf. Proc. 1489 (2012) 178.
[21] G. Hautier, A. Jain, Sh. Ping Ong, B. Kang, Ch. Moore, R. Doe, G. Ceder, Phosphates as lithium-ion battery cathodes: an evaluation based on high-throughput ab Initio calculations, Chem. Mater. 23 (2011) 3495.
[22] A.V. Chadwick, J. Corish, Defects and matter transport in solid materials, in: C.R.A. Catlow, A. Cheetham (Eds.), New trends in Materials Chemistry, Kluwer Academic Publishers, Netherlands, 1997, p. 285.